

# High fidelity state preparation and measurement of ion hyperfine qubits with $I > \frac{1}{2}$

Fangzhao Alex An,<sup>1,\*</sup> Anthony Ransford,<sup>2,†</sup> Andrew Schaffer,<sup>1</sup> Lucas R. Sletten,<sup>1</sup> John Gaebler,<sup>2</sup> James Hostetter,<sup>1</sup> and Grahame Vittorini<sup>1</sup>

<sup>1</sup>Quantinuum, Golden Valley, MN, USA

<sup>2</sup>Quantinuum, Broomfield, CO, USA

(Dated: March 4, 2022)

We present a method for achieving high fidelity state preparation and measurement (SPAM) using trapped ion hyperfine qubits with nuclear spins higher than  $I = 1/2$ . The ground states of these higher nuclear spin isotopes do not afford a simple frequency-selective state preparation scheme. We circumvent this limitation by stroboscopically driving strong and weak transitions, blending fast optical pumping using E1 transitions and narrow microwave or optical E2 transitions. We demonstrate this method with the  $I = 3/2$  isotope  $^{137}\text{Ba}^+$  to achieve a SPAM infidelity of  $9.6(1.4) \times 10^{-5}$  ( $-40.2(0.6)$  dB), facilitating the use of a wider range of ion isotopes with favorable wavelengths and masses for quantum computation.

## INTRODUCTION

State preparation and measurement (SPAM) is fundamental to quantum computation and covers two of the five necessary DiVincenzo criteria [1]. Modern quantum systems are not error corrected, and the fidelity of an uncorrected  $N$ -qubit register typically decreases exponentially with size as  $(\mathcal{F}_{\text{SPAM}})^N$ , where  $\mathcal{F}_{\text{SPAM}}$  is the single-qubit SPAM fidelity. Currently implemented error correction codes require mid-circuit measurement and reset (MCMR) and thus SPAM errors contribute to the error correction budget as the ratio of gates to measurements [2]. Given the historic difficulty of improving gate fidelity, it will likely be desirable to make the SPAM contribution negligible and thus on par with the gate fidelity. Moreover, the speed at which SPAM can be performed can affect memory errors during MCMR, and the compatibility of the exact SPAM technique with other qubit operations must also be considered. More broadly, it is desirable to have fast, high-fidelity SPAM in ionic qubits with other practical advantages to quantum computation such as light mass and visible wavelengths for gates.

Although the  $^{171}\text{Yb}^+$  ion boasts a hyperfine clock qubit and its  $I = 1/2$  nuclear spin affords it a singlet state for simple, high fidelity state preparation [3, 4], the limitations on measurement fidelity, necessity for high power UV light, and associated photo-induced charging [5] present significant engineering challenges. Other systems with similar structure (nuclear spin  $I = 1/2$ ) have been explored, with the most promising being  $^{133}\text{Ba}^+$  [6, 7] due to its visible wavelength transitions, but these species either require lasers deep in the UV or are not naturally occurring, presenting formidable challenges for scaling systems.

Despite their complicated structure, ions with nuclear spin  $I > 1/2$  have advantages [9] and are used in quantum information and quantum computing, including  $^9\text{Be}^+$  [10],  $^{43}\text{Ca}^+$  [11],  $^{25}\text{Mg}^+$  [12] and  $^{137}\text{Ba}^+$  [13]. Currently, all methods of state preparation in these species

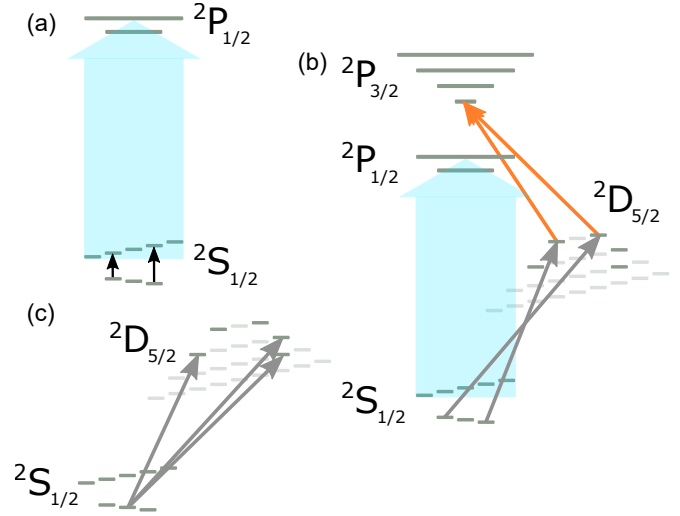


FIG. 1. (a) Microwave-assisted optical pumping (MAOP) using coherent microwave pulses (black) and 493 nm flush pulses (aqua). (b) 1762 nm narrow-band optical pumping (NBOP) using coherent 1762 nm pulses (gray), 614 nm quenching (orange), and 493 nm flush (aqua). (c) Cabinet shelving with repeated 1762 nm pulses addressing  $|0\rangle$ . Hyperfine quantum numbers  $F$  and  $m_F$  are omitted for clarity (see Supplementary Materials for detailed labeling and timing diagram [8]).

are limited in performance by their requirement for either light with high polarization purity or a series of coherent gate operations to map a prepared state to the clock qubit state, where this transfer infidelity shows up as a preparation error [10, 14].

In this work, we prepare a single  $^{137}\text{Ba}^+$  ion into the qubit state  $|0\rangle \equiv |6S_{1/2}, F=1, m_F=0\rangle$  without the need of highly polarized light or coherent mapping of the qubit to the clock state. By alternating between standard optical pumping on a dipole transition and driving narrow, state-selective microwave or optical E2 transitions, we are able to address and minimize the state preparation error in the Zeeman sublevels of the ground state  $6S_{1/2}$ .

Species	$I$	$\eta_{F'+1, F+1}$	$\eta_{F', F+1}$	$\frac{\Gamma}{2\pi}$ (MHz)	Hyperfine S (GHz)	Hyperfine P (GHz)	$\epsilon_{\text{prep}}$
$^9\text{Be}^+$	3/2	1/2	5/6	22.4 [15]	1.25 [16]	0.194 [17]	5.4e-4
$^{25}\text{Mg}^+$	5/2	4/9	7/9	42.4 [18]	1.788 [18]	0.307 [18]	1.0e-3
$^{43}\text{Ca}^+$	7/2	5/12	3/4	22.4 [19]	3.226 [20]	0.581 [20]	8.9e-5
$^{87}\text{Sr}^+$	9/2	2/5	11/15	21.5 [21]	5.0 [22]	0.89 [22]	3.4e-5
$^{135}\text{Ba}^+$	3/2	1/2	5/6	20.1 [23]	7.18 [24]	1.33 [24]	1.4e-5
$^{137}\text{Ba}^+$	3/2	1/2	5/6	20.1 [23]	8.03 [13]	1.49 [13]	1.1e-5
$^{173}\text{Yb}^+$	5/2	4/9	7/9	19.7 [25]	10.5 [26]	1.85 [27]	6.3e-6

TABLE I. Predicted state preparation infidelities in commonly used ion species. The infidelity generally decreases with mass with the exception of  $^{25}\text{Mg}^+$ , which has a transition linewidth that is two times broader.

This technique, generalizable to many  $I > 1/2$  species, allows us to achieve the highest SPAM fidelity recorded with any qubit to the best of our knowledge (previously  $^{171}\text{Yb}^+$  [28]).

We present two varieties of the state preparation scheme, both of which are cyclic in nature and seek to reduce state preparation errors in all Zeeman sublevels of  $S_{1/2}$  except  $|0\rangle$ . The microwave scheme is shown in Fig. 1(a), and is similar to the microwave-assisted optical pumping (MAOP) recently performed on an atomic ensemble [29]. We first use dipole optical pumping at 493 nm to “flush” out errors from the  $(S_{1/2}, F = 2)$  manifold, redistributing the errors in the Zeeman sublevels of  $(S_{1/2}, F = 1)$ . Next, errors in the non-qubit Zeeman sublevels of the  $(S_{1/2}, F = 1)$  manifold are moved up to  $F = 2$  with microwave  $\pi$ -pulses near the hyperfine splitting, and are subsequently flushed by the 493 nm light when the cycle repeats. Alternatively, the errors in  $(S_{1/2}, F = 1)$  can be addressed with narrow-band optical pumping (NBOP) [28] to  $D_{5/2}$  on the 1762 nm E2 transition, and then redistributed back into the  $(S_{1/2}, F = 1)$  manifold with a 614 nm pulse (Fig. 1(b)).

State preparation with either MAOP or NBOP can be generalized to different ion species with high nuclear spin, and we model MAOP state preparation for a general alkaline earth ion with a dipole transition from S (hyperfine states  $F, F + 1$ ) to P ( $F', F' + 1$ ) [8]. In the limit of many cycles and low flush beam power, we derive the state preparation error to be

$$\epsilon_{\text{prep}} = \frac{\Gamma^2}{2} \left[ \frac{1}{\delta_{\text{HF}, S}^2} + \frac{\eta_{F', F+1}}{\eta_{F'+1, F+1}} \frac{1}{\delta_-^2} \right], \quad (1)$$

where  $\Gamma$  is the transition linewidth,  $\delta_{\text{HF}, S}$  is the ground state hyperfine splitting, and  $\eta_{i,j}$  denotes the branching from state  $i$  to state  $j$ . The first term is identical to twice the limit of state preparation in an  $I = 1/2$  ion and the second term is a correction factor that depends on the branching ratio and hyperfine splitting difference between the ground and excited states  $\delta_-$ . The parameters for Eq. (1) and the associated fidelities for various  $I > 1/2$  hyperfine qubits are shown in Table I.

There are a variety of high fidelity measurement

schemes in general from quantum logic and quantum non-demolition [30] to coherent and incoherent shelving. For  $^{137}\text{Ba}^+$  we use a “cabinet shelving” procedure shown in Fig. 1(c) where  $|0\rangle$  is shelved three times in succession to multiple Zeeman sublevels in the metastable  $D_{5/2}$  state (30 s lifetime [31]), and then we apply resonant 493 nm light for 350  $\mu\text{s}$  to detect fluorescence. The resulting bright and dark state histograms are well separated and the SPAM infidelity for the 1762 nm scheme is measured to be  $9.6(1.4) \times 10^{-5}$  with a simple discriminator (Fig. 2(c)). The data is taken without any pre- or post-processing, such as discarding trials based on low fluorescence counts during Doppler cooling. We do not perform statistical detection of D-state decays for our SPAM fidelity [15], but consider the effect in the error budget.

In this experiment, we trap single  $^{137}\text{Ba}^+$  ions 70  $\mu\text{m}$  above a planar surface trap similar to that described in Ref. [32], and apply a magnetic field of 4.96 G to define the quantization axis. Single qubit rotations between the states  $|0\rangle$  and  $|1\rangle \equiv |S_{1/2}, 2, 0\rangle$  are driven by a microwave horn tuned near the transition frequency of 8.038 GHz. The ion is Doppler cooled by cycling through the  $S_{1/2} \leftrightarrow P_{1/2}$  (493 nm cycling) and  $D_{3/2} \leftrightarrow P_{1/2}$  (650 nm repump) transitions. To address the many hyperfine levels of  $^{137}\text{Ba}^+$ , frequency sidebands are applied to all of our lasers with electro-optic modulators (EOMs) [8]. The 493 nm cycling light is wavemeter locked to the  $F = 2 \leftrightarrow F = 2$  ( $2 \leftrightarrow 2$ ) hyperfine transition, and an EOM applies sidebands to address the other possible hyperfine transitions ( $1 \leftrightarrow 1$ ,  $1 \leftrightarrow 2$ , and  $2 \leftrightarrow 1$ ). For state preparation and measurement, we address the narrow shelving transition  $S_{1/2} \leftrightarrow D_{5/2}$  with a 1762 nm laser locked to a high-finesse optical cavity. This laser is red-detuned by 88 MHz from the  $|S_{1/2}, 1, 0\rangle \rightarrow |D_{5/2}, 3, 2\rangle$  transition to avoid off-resonant shelving, and different shelving transitions are addressed with sidebands generated by an EOM. A 614 nm laser is used to deshelve ions from  $D_{5/2}$  to  $P_{3/2}$ , from which ions preferentially fall into  $S_{1/2}$ .

We begin our state preparation with a fast (40  $\mu\text{s}$ ) polarization-limited step. We address the  $(S_{1/2}, F =$

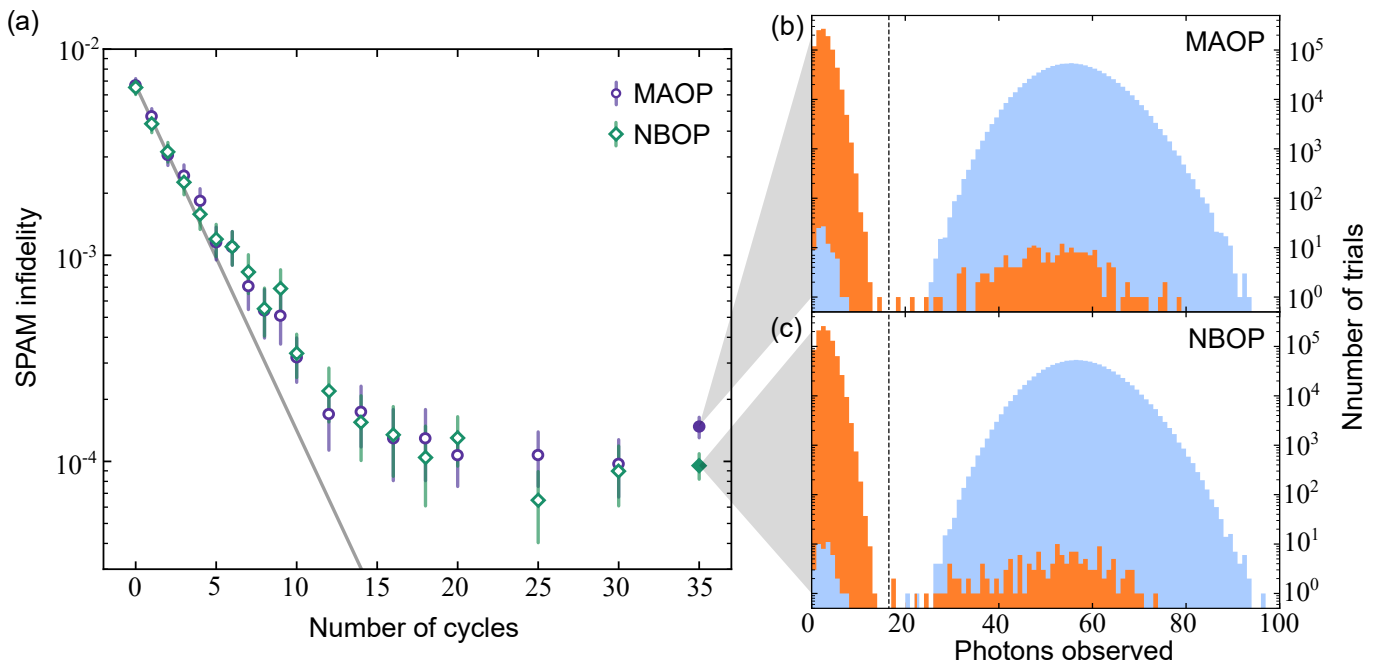


FIG. 2. (a) SPAM infidelity vs. increasing cycles of microwave-assisted (purple, MAOP) and narrow-band (green, NBOP) optical pumping. Infidelities are calculated from datasets with  $50 \times 10^3$  (for 0 to 9 cycles),  $100 \times 10^3$  (10 to 18 cycles), and  $200 \times 10^3$  (20 to 30 cycles) trials. Both techniques are initially close to  $1/3$  reduction in error per cycle (gray line), but level off at high fidelity. Solid points and fluorescence count histograms represent separate datasets for (b) MAOP (35 cycles) and (c) 1762 nm NBOP (30 cycles with 493 nm flush pulse and 5 cycles without flush), preparing the  $|0\rangle$  (orange) and  $|1\rangle$  (blue) qubit state over  $10^6$  trials per state. The SPAM infidelities were measured to be  $(14.8 \pm 1.7) \times 10^{-5}$  (microwaves) and  $(9.6 \pm 1.4) \times 10^{-5}$  (1762 nm) using state detection thresholds indicated by vertical lines. All error bars denote one Wilson interval.

$2) \rightarrow (P_{1/2}, F = 2)$  transition with  $\pi$ -polarized 493 nm light and stroboscopically apply sidebands to address the  $2 \leftrightarrow 1$  and  $1 \leftrightarrow 1$  transitions (see Supplementary Materials for exact pulse sequences [8]). Because of the forbidden selection rule  $|S_{1/2}, 1, 0\rangle \leftrightarrow |P_{1/2}, 1, 0\rangle$ , this stochastically pumps the population into the qubit  $|0\rangle$  state. The stroboscopic pulsing prevents frequency mixing of the sidebands by the EOM which drives the unwanted  $1 \leftrightarrow 2$  transition and could thus drive population out of the  $|0\rangle$  state. This process typically achieves state preparation infidelities of  $\sim 7 \times 10^{-3}$ , where the fidelity is limited by polarization impurities and the laser orientation with respect to the magnetic field [8]. While one could attempt to improve these imperfections, it is technically difficult given vacuum window birefringence, finite quality retarders, and incomplete magnetic field control, all of which will be further exacerbated in a larger system with many spatially-separated qubits.

After polarization-limited state preparation, some unwanted population is left as error in the remaining Zeeman sublevels of  $S_{1/2}$ . To flush out the leakage population in the  $F = 2$  manifold, we apply a weak pulse ( $1 \mu\text{s}$ ,  $40 \text{ mW/cm}^2$ ) of 493 nm light carrying all polarizations and tuned to  $(S_{1/2}, F = 2) \rightarrow (P_{1/2}, F = 2)$  to pump population equally into the three Zeeman sublevels of  $(S_{1/2}, F = 1)$ . During this pulse, 650 nm light is also ap-

plied to pump population out of the  $D_{3/2}$  manifold. Next, to address the leakage population in  $|S_{1/2}, 1, \pm 1\rangle$ , we can use either microwave pulses to  $|S_{1/2}, 2, \pm 1\rangle$  or shelving pulses to  $|D_{5/2}, 1, \mp 1\rangle$ . Under MAOP, two successive  $\pi$ -pulses  $|S_{1/2}, 1, \pm 1\rangle \rightarrow |S_{1/2}, 2, \pm 1\rangle$  ( $\sim 50 \mu\text{s}$ ) are applied to bring population into  $F = 2$  in preparation for another 493 nm flush pulse. Each cycle of this procedure should ideally transfer the errors out of  $F = 1, m_F = \pm 1$  with microwaves, and then redistribute those errors equally back into the  $F = 1$  manifold with the 493 nm flush pulse, leading to a  $1/3$  reduction in error per cycle. Since the microwave transitions are well separated from other transitions at our Rabi rates ( $2\pi \times 10 \text{ kHz}$ ), off-resonant excitations of the qubit state by the 493 nm enforce a more fundamental limit.

For NBOP, we apply two  $\pi$ -pulses of 1762 nm light  $|S_{1/2}, 1, \pm 1\rangle \rightarrow |D_{5/2}, 1, \mp 1\rangle$  ( $45, 55 \mu\text{s}$ ) to pump error into the  $D_{5/2}$  state. The orientation and polarization of the 1762 nm laser allows for only  $\Delta m_F = \pm 2$  transitions, meaning that any accidental shelving of the qubit state is suppressed by frequency separation, polarization, and laser  $k$ -vector. Next, we apply a  $4 \mu\text{s}$  pulse of 614 nm light to address the dipole transition  $(D_{5/2}, F = 1) \rightarrow (P_{3/2}, F = 0)$ , from which population decays to the  $F = 1$  of the  $S_{1/2}$  state with branching 73.8% (zero branching to  $F = 2$ ) [33]. To address any population that falls back

Error Source	Predicted Error ( $\times 10^{-5}$ )	
	$ 0\rangle$ State	$ 1\rangle$ State
$ 0\rangle$ state preparation	$<9.1$	—
$ 0\rangle \rightarrow  1\rangle$ transfer	—	$5.4 \pm 0.5$
Shelving infidelity	$\sim 0.1$	—
$D_{5/2}$ decay	$\sim 1.5$	—
Correlated errors	4.0	—
Subtotal (measured)	$14.7 \pm 2.4$	$4.2 \pm 1.3$
Total (measured)	$9.6 \pm 1.4$	

TABLE II. Error budget for 1762 nm narrow-band optical pumping SPAM results of Fig. 2(c).

into  $D_{5/2}$ , we apply sidebands to the 614 nm light that march the population to ( $P_{3/2}, F = 0$ ):  $2 \rightarrow 1$ ,  $3 \rightarrow 2$ , and  $4 \rightarrow 3$ . Similarly, 650 nm light is applied to repump population that falls into  $D_{3/2}$ . In contrast to MAOP, this scheme does not explicitly pump population into the ( $S_{1/2}, F = 2$ ) manifold, so we need not apply the 493 nm  $F = 2$  flush beam as frequently, lowering the error from 493 nm off-resonant excitations.

To characterize SPAM fidelity, we must also prepare  $|1\rangle \equiv |S_{1/2}, 2, 0\rangle$  by applying a composite microwave  $\pi$ -pulse (CP Robust 180 sequence [6, 34]) at the qubit frequency after preparing  $|0\rangle$ . To distinguish between the two qubit states, we cabinet shelve population in  $|0\rangle$  with three  $\pi$ -pulses to the states  $|D_{5/2}, 3, 2\rangle$ ,  $|D_{5/2}, 2, \pm 2\rangle$  (165, 45, 55  $\mu$ s). Each of these pulses is limited to a fidelity of only  $\sim 0.99$  due to magnetic field and laser intensity noise, but with three pulses we are able to shelve with an implied infidelity of  $1 \times 10^{-6}$ . After shelving, 493 nm and 650 nm light are applied with all sidebands to detect any population in  $S_{1/2}$ ,  $P_{1/2}$ , and  $D_{3/2}$ .

Figure 2(a) presents the SPAM performance of both state preparation procedures over a variable number of cycles including the 493 nm flush beam. After  $>25$  cycles of either MAOP or NBOP, we observe a drop in the SPAM infidelity of nearly two orders of magnitude compared to using polarization state preparation alone. Both state preparation schemes initially exhibit close to the expected 1/3 reduction in error (gray line), but poor shelving due to ion heating as well as off-resonant scattering errors from the 493 nm flush beam cause the performance to deviate at large cycle number.

The performance of MAOP and NBOP appear comparable up until 30 cycles with the flush pulse, but the 1762 nm scheme proves superior in a larger dataset ( $10^6$  trials) at 35 cycles, where we omit the 493 flush pulse in the final five cycles of NBOP. The fluorescence count histograms for this 35 cycle data are shown in Fig. 2(b-c), and using the same discriminator (vertical dashed line) we extract SPAM infidelities of  $(1.48 \pm 0.17) \times 10^{-4}$  (MAOP) and  $(9.6 \pm 1.4) \times 10^{-5}$  (NBOP). We examine the SPAM errors of the higher fidelity NBOP result in more

detail in Table II. Some errors are caused by shelved ions spontaneously decaying from the  $D_{5/2}$  state into states bright to the measurement light, and these can be reduced by shortening our measurement time and increasing the shelving Rabi rates. The majority of the errors that occur when preparing  $|1\rangle$  are due to an imperfect microwave transfer pulse between  $|0\rangle$  and  $|1\rangle$ , and we find that they are within error of an independent measurement of the microwave infidelity  $(5.4 \pm 0.5) \times 10^{-5}$  using single-qubit randomized benchmarking [35]. Other errors include collision-induced correlated errors which we detail further in the Supplementary Materials [8].

Our present implementation of these state preparation techniques takes about 3.5 ms for 35 cycles using  $\sim 50 \mu$ s microwave and 1762 nm  $\pi$ -times. These long durations can result in hot ions, limiting achievable fidelities mainly through failed  $D_{5/2}$  state shelving. Moreover, this timescale is significantly longer than typical ion qubit gate times of 50  $\mu$ s, impacting overall circuit runtime. We can reduce the required time for either scheme by performing both  $\pi$ -pulses in parallel. Furthermore, if we allow an error of  $10^{-5}$  due to off-resonant excitation of  $|0\rangle$ , then the minimum allowed microwave and 1762 nm  $\pi$ -times are 12.5  $\mu$ s and 2.5  $\mu$ s, respectively. We project that these improvements could cut down the state preparation time to 450  $\mu$ s (microwave) and 250  $\mu$ s (1762 nm).

In this work, we have achieved the highest reported SPAM fidelity of any qubit using a  $^{137}\text{Ba}^+$  ion with nuclear spin  $I = 3/2$ . Our two similar state preparation techniques are generalizable to many ion species with higher nuclear spin  $I > 1/2$ , facilitating quantum computation with new ion species with benefits like visible wavelengths and lighter masses.

The authors would like to thank Stephen Erickson, Chris Gilbreth, Colin Kennedy, Conrad Roman, and Jonathan Sedlacek for their suggestions and advice, as well as the rest of the Quantinuum team for their contributions.

\* Fangzhao.An@Quantinuum.com

† Anthony.Ransford@Quantinuum.com

- [1] D. P. DiVincenzo, *Fortschr. Phys.* **48**, 771 (2000).
- [2] C. Ryan-Anderson, J. G. Bohnet, K. Lee, D. Gresh, A. Hankin, J. P. Gaebler, D. Francois, A. Chernoguzov, D. Lucchetti, N. C. Brown, T. M. Gatterman, S. K. Halit, K. Gilmore, J. A. Gerber, B. Neyenhuis, D. Hayes, and R. P. Stutz, *Phys. Rev. X* **11**, 041058 (2021).
- [3] S. Olmschenk, K. C. Younge, D. L. Moehring, D. N. Matsukevich, P. Maunz, and C. Monroe, *Phys. Rev. A* **76**, 052314 (2007).
- [4] S. Crain, C. Cahall, G. Vrijsen, E. E. Wollman, M. D. Shaw, V. B. Verma, S. W. Nam, and J. Kim, *Commun. Phys.* **2**, 97 (2019).
- [5] S. X. Wang, G. Hao Low, N. S. Lachenmyer, Y. Ge, P. F. Herskind, and I. L. Chuang, *J. Appl. Phys.* **110**, 104901

- (2011).
- [6] J. E. Christensen, D. Hucul, W. C. Campbell, and E. R. Hudson, *npj Quantum Inf.* **6**, 35 (2020).
- [7] P. J. Lee, *Quantum information processing with two trapped cadmium ions*, Ph.D. thesis, University of Michigan (2006).
- [8] See the Supplementary Materials for more detailed level diagram of  $^{137}\text{Ba}^+$ , derivation of state preparation error, details on initial polarization state preparation, specifics on SPAM error budget, and timing diagrams for state preparation techniques.
- [9] D. T. C. Allcock, W. C. Campbell, J. Chiaverini, I. L. Chuang, E. R. Hudson, I. D. Moore, A. Ransford, C. Roman, J. M. Sage, and D. J. Wineland, *Appl. Phys. Lett.* **119**, 214002 (2021).
- [10] J. P. Gaebler, T. R. Tan, Y. Lin, Y. Wan, R. Bowler, A. C. Keith, S. Glancy, K. Coakley, E. Knill, D. Leibfried, and D. J. Wineland, *Phys. Rev. Lett.* **117**, 060505 (2016).
- [11] C. J. Ballance, T. P. Harty, N. M. Linke, M. A. Sepiol, and D. M. Lucas, *Phys. Rev. Lett.* **117**, 060504 (2016).
- [12] T. R. Tan, J. P. Gaebler, Y. Lin, Y. Wan, R. Bowler, D. Leibfried, and D. J. Wineland, *Nature* **528**, 380 (2015).
- [13] M. R. Dietrich, N. Kurz, T. Noel, G. Shu, and B. B. Blinov, *Phys. Rev. A* **81**, 052328 (2010).
- [14] T. P. Harty, D. T. C. Allcock, C. J. Ballance, L. Guidoni, H. A. Janacek, N. M. Linke, D. N. Stacey, and D. M. Lucas, *Phys. Rev. Lett.* **113**, 220501 (2014).
- [15] C. E. Langer, *High fidelity quantum information processing with trapped ions*, Ph.D. thesis, University of Colorado at Boulder (2006).
- [16] D. J. Wineland, J. J. Bollinger, and W. M. Itano, *Phys. Rev. Lett.* **50**, 628 (1983).
- [17] J. J. Bollinger, J. S. Wells, D. J. Wineland, and W. M. Itano, *Phys. Rev. A* **31**, 2711 (1985).
- [18] J. Nguyen, *The linewidth and hyperfine A constant of the  $^2P_{1/2}$  state of a magnesium ion confined in a linear Paul trap*, Ph.D. thesis, McMaster University (2009).
- [19] D. F. V. James, *Appl. Phys. B* **66**, 181 (1998).
- [20] D. M. Lucas, A. Ramos, J. P. Home, M. J. McDonnell, S. Nakayama, J.-P. Stacey, S. C. Webster, D. N. Stacey, and A. M. Steane, *Phys. Rev. A* **69**, 012711 (2004).
- [21] E. H. Pinnington, R. W. Berends, and M. Lumsden, *J. Phys. B: At. Mol. Opt. Phys.* **28**, 2095 (1995).
- [22] X. Yuan, S. N. Panigrahy, R. W. Dougherty, T. P. Das, and J. Andriessen, *Phys. Rev. A* **52**, 197 (1995).
- [23] J. Christensen, *High-fidelity operation of a radioactive trapped-ion qubit  $^{133}\text{Ba}^+$* , Ph.D. thesis, University of California Los Angeles (2020).
- [24] P. Villemoes, A. Arnesen, F. Hejlskov, and A. Wannstrom, *J. Phys. B: At. Mol. Opt. Phys.* **26**, 4289 (1993).
- [25] S. Olmschenk, D. Hayes, D. N. Matsukevich, P. Maunz, D. L. Moehring, K. C. Younge, and C. Monroe, *Phys. Rev. A* **80**, 022502 (2009).
- [26] A. Münch, M. Berkler, C. Gerz, D. Wilsdorf, and G. Werth, *Phys. Rev. A* **35**, 4147 (1987).
- [27] C. H. Roman, *Expanding the  $^{171}\text{Yb}^+$  toolbox: the  $^2F_{7/2}^o$  state as resource for quantum information science*, Ph.D. thesis, University of California Los Angeles (2021).
- [28] A. Ransford, C. Roman, T. Dellaert, P. McMillin, and W. C. Campbell, *Phys. Rev. A* **104**, L060402 (2021).
- [29] A. Tretiakov, C. Potts, Y. Lu, J. Davis, and L. LeBlanc, *arXiv preprint arXiv:2110.10673* (2021).
- [30] S. D. Erickson, J. J. Wu, P.-Y. Hou, D. C. Cole, S. Geller, A. Kwiatkowski, S. Glancy, E. Knill, D. H. Slichter, A. C. Wilson, *et al.*, *arXiv preprint arXiv:2112.06341* (2021).
- [31] Z. Zhang, K. J. Arnold, S. R. Chanu, R. Kaewuam, M. S. Safronova, and M. D. Barrett, *Phys. Rev. A* **101**, 062515 (2020).
- [32] J. M. Pino, J. M. Dreiling, C. Figgatt, J. P. Gaebler, S. A. Moses, M. S. Allman, C. H. Baldwin, M. Foss-Feig, D. Hayes, K. Mayer, C. Ryan-Anderson, and B. Neyenhuis, *Nature* **592**, 209 (2021).
- [33] T. Dutta, D. De Munshi, D. Yum, R. Rebhi, and M. Mukherjee, *Sci. Rep.* **6**, 29772 (2016).
- [34] C. A. Ryan, J. S. Hodges, and D. G. Cory, *Phys. Rev. Lett.* **105**, 200402 (2010).
- [35] E. Knill, D. Leibfried, R. Reichle, J. Britton, R. B. Blakestad, J. D. Jost, C. Langer, R. Ozeri, S. Seidelin, and D. J. Wineland, *Phys. Rev. A* **77**, 012307 (2008).

# High fidelity state preparation and measurement of ion hyperfine qubits with $I > \frac{1}{2}$

Fangzhao Alex An,<sup>1,\*</sup> Anthony Ransford,<sup>2,†</sup> Andrew Schaffer,<sup>1</sup> Lucas R. Sletten,<sup>1</sup> John Gaebler,<sup>2</sup> James Hostetter,<sup>1</sup> and Grahame Vittorini<sup>1</sup>

<sup>1</sup>Quantinuum, Golden Valley, MN, USA

<sup>2</sup>Quantinuum, Broomfield, CO, USA

(Dated: March 4, 2022)

## ENERGY LEVEL DIAGRAM OF $^{137}\text{Ba}^+$

Figure S1 shows the level structure of  $^{137}\text{Ba}^+$  and the transitions we address in this work. We deal with the many hyperfine levels by applying frequency sidebands to all of our lasers using electro-optic modulators. The relevant Zeeman levels in  $^2\text{D}_{5/2}$  are highlighted: we shelve from  $|0\rangle$  to  $|D_{5/2, 2, \pm 2}\rangle$  and  $|D_{5/2, 3, 2}\rangle$ , and we use  $|S_{1/2, 1, \pm 1}\rangle \rightarrow |D_{5/2, 1, \mp 1}\rangle$  for 1762 nm narrow-band optical pumping.

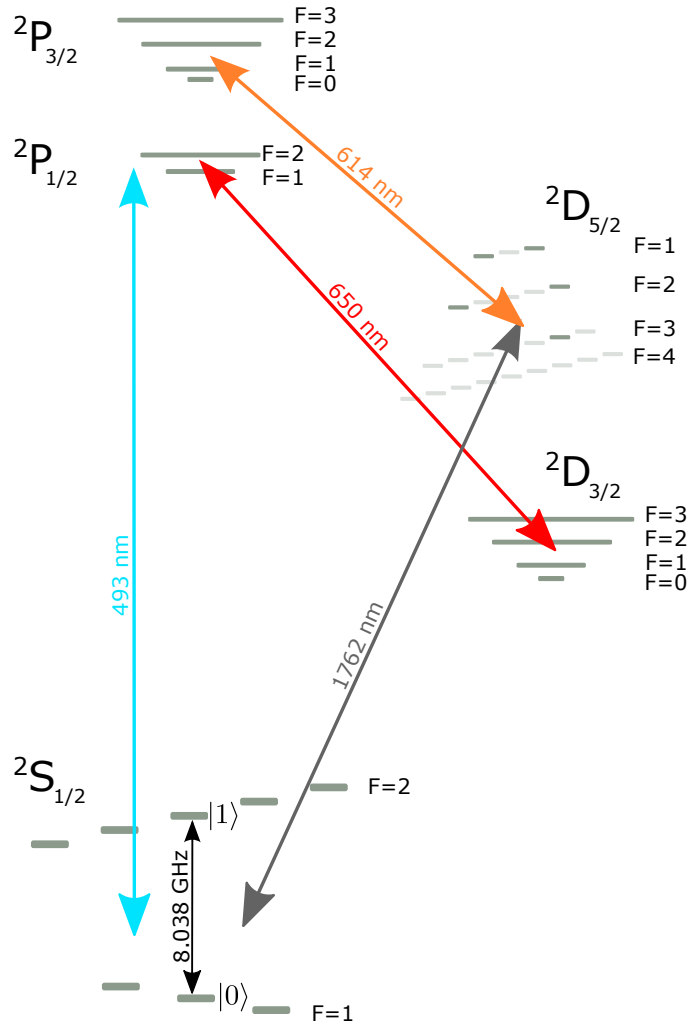


**Figure S1.** Level diagram of  $^{137}\text{Ba}^+$  highlighting the transitions addressed in this work: 493 nm cycling (aqua), 650 nm repump (red), 1762 nm shelving (gray), 614 nm deshelling (orange), and microwave transition between  $^2\text{S}_{1/2}$  hyperfine levels (black).

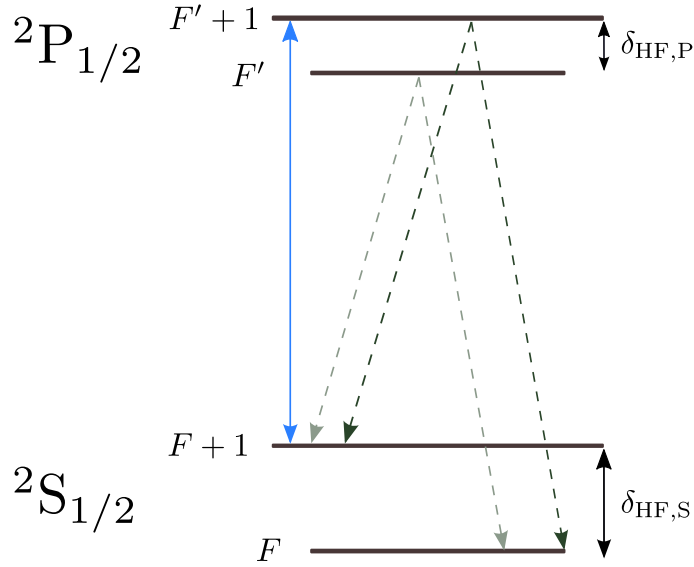


**Figure S2.** Level diagram of a typical alkaline earth ion with flush pulse (blue), flush branching (dark dashed lines) and error branching (light dashed lines).

### MODELING MICROWAVE-ASSISTED OPTICAL PUMPING STATE PREPARATION

We consider a general alkaline earth ion with a level structure shown in Fig. S2. Under our microwave state preparation technique, the flushing laser addresses the  $F + 1 \rightarrow F' + 1$  transition, fully clearing out the  $F + 1$  manifold. Microwaves tuned near the hyperfine splitting  $\delta_{\text{HF},S}$  then drive population from the unwanted Zeeman states in the  $F$  manifold to the  $F + 1$  manifold, and the cycle is repeated. In the limit of low flush power and a large number of pulses, the steady state can be viewed as equal populations in the upper ( $F + 1$ ) and lower ( $F$ ) manifold Zeeman states. The time rate of change of the non-qubit Zeeman states is given by

$$\frac{d\rho_{\neq|0\rangle}}{dt} = \eta_{F'+1,F} \frac{\gamma}{2} \rho_{\neq|0\rangle}, \quad (\text{S1})$$

and the rate equation for the qubit state is given by

$$\frac{d\rho_{|0\rangle}}{dt} = \left[ \eta_{F'+1,F+1} \left( \frac{\Gamma}{2\delta_{\text{HF},S}} \right)^2 + \eta_{F',F+1} \left( \frac{\Gamma}{2\delta_-} \right)^2 \right] \gamma \rho_{|0\rangle}, \quad (\text{S2})$$

where  $\eta_{i,j}$  denotes the branching from state  $i$  to state  $j$ ,  $\gamma$  is the scattering rate,  $\Gamma$  is the transition linewidth, and  $\delta_- = \delta_{\text{HF},S} - \delta_{\text{HF},P}$  is the difference of the hyperfine splittings. The factor of 2 in Eq. (S1) comes from the steady state assumption of equal population in the two coupled Zeeman states. Setting these rates equal to each other, we solve for the steady state and take the ratio of the populations as the state preparation error

$$\epsilon_{\text{prep}} = \frac{\Gamma^2}{2} \left[ \frac{1}{\delta_{\text{HF},S}^2} + \frac{\eta_{F',F+1}}{\eta_{F'+1,F+1}} \frac{1}{\delta_-^2} \right]. \quad (\text{S3})$$

The first term is identical to twice the limit of state preparation in an  $I = 1/2$  ion and the second term is a correction factor that depends on the branching ratio and hyperfine splitting difference between the ground and excited states  $\delta_-$ . The parameters for Eq. (S3) and the associated fidelities for various  $I > 1/2$  hyperfine qubits are shown in Table I of the main text. We do not model the measurement errors in general because of the variety of high fidelity schemes available from coherent and incoherent shelving to quantum logic and quantum non-demolition [1].

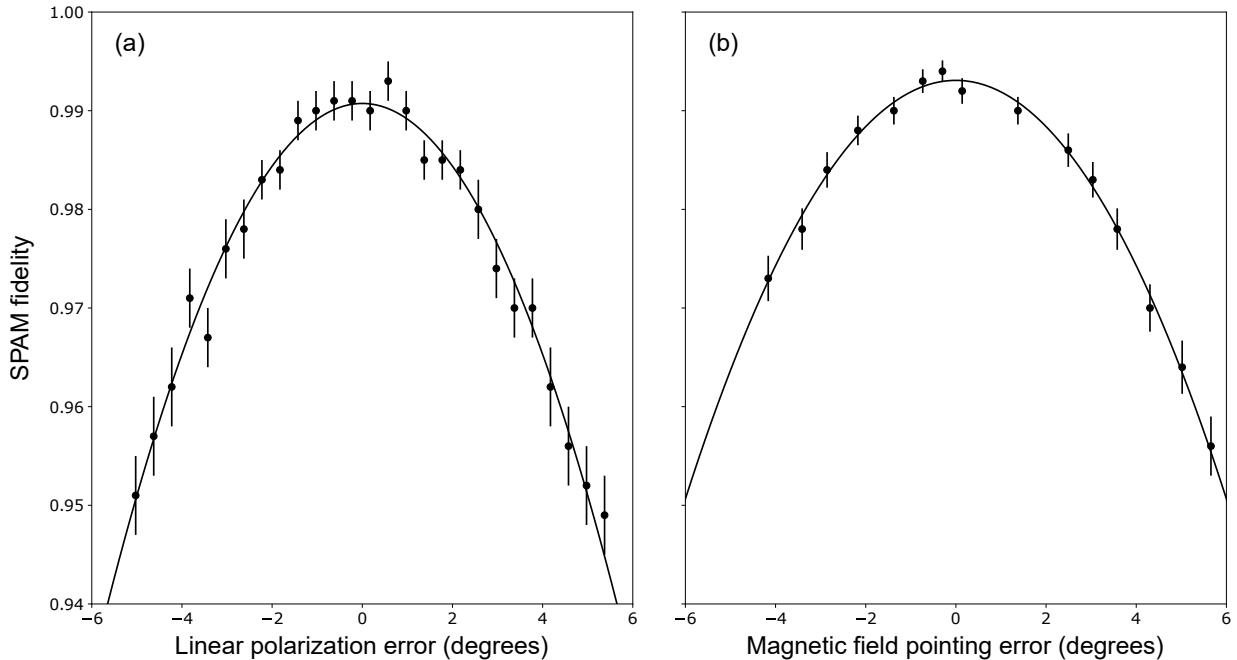


**Figure S3.** Errors in polarization SPAM can be exacerbated by (a) polarization errors in the optical pumping beam, shown here as a rotation of the linear polarization, or (b) incorrect alignment of the magnetic field to the  $k$ -vector, demonstrated here using orthogonal magnetic field shims. Lines are added to guide the eye.

### POLARIZATION STATE PREPARATION

Using polarization state preparation alone, we can achieve SPAM infidelities of  $(5.5 \pm 1.5) \times 10^{-3}$ . The fundamental limit is off-resonant excitation of  $|0\rangle$ , but we believe this fidelity is technically limited by polarization impurities and imperfect alignment of the laser  $k$ -vector orthogonal to the quantization axis. To investigate these error mechanisms, we measured the infidelity as a function both magnetic field direction and polarization (Fig. S3). To vary the magnetic field direction, we measured SPAM fidelity while applying a shim field using coils orthogonally polarized to the quantization axis, recalibrating our shelving transitions to account for any changes to overall magnetic field amplitude. To introduce polarization impurities, we simply rotated a half-wave plate before measuring SPAM fidelity. While one could attempt to further improve these imperfections, it is technically difficult given vacuum window bi-refringence, finite quality retarders, and incomplete magnetic field control, all of which will be further complicated in a system with many spatially separated qubits. Though we found optimal performance at a non-zero shim field, the coils were ultimately disconnected to reduce any magnetic field noise introduced to the shelving transitions and further SPAM improvements were achieved using the techniques described in the main text.

### ERROR BUDGET FOR 1762 NM NARROW-BAND OPTICAL PUMPING SPAM

Here we describe in more detail the errors in our measured SPAM infidelity using 1762 nm narrow-band optical pumping, reproduced in Table S-i above. As described in the main text, we use an imperfect microwave composite  $\pi$ -pulse to prepare  $|1\rangle$  from  $|0\rangle$ , and we estimate its infidelity by performing single-qubit randomized benchmarking to get a simple  $\pi$ -pulse infidelity of  $(5.4 \pm 0.5) \times 10^{-5}$ . We believe that this is caused in part by some low frequency noise that causes our microwave  $\pi$ -times to drift over the course of our dataset. This is within error of our measured  $|1\rangle$  preparation errors.

Some errors arise from ions decaying from the shelved state  $D_{5/2}$  during measurement ( $350 \mu\text{s}$ ) as well as cabinet shelving itself (three  $\pi$ -pulses:  $165 \mu\text{s}$ ,  $45 \mu\text{s}$ , and  $55 \mu\text{s}$ ). Given the 30.1 s lifetime of the  $D_{5/2}$  state [2], the error from decays ranges from  $1.16 \times 10^{-5}$  (considering only measurement time) to  $2.04 \times 10^{-5}$  (considering full cabinet shelving and measurement). In post-processing, we are able to identify a portion of the decays that actually occurred because the  $350 \mu\text{s}$  measurement time was recorded in ten  $35 \mu\text{s}$  intervals, and an accidentally bright error caused by a decay will register few counts in early segments before becoming bright in later ones. We analyzed the measurements using

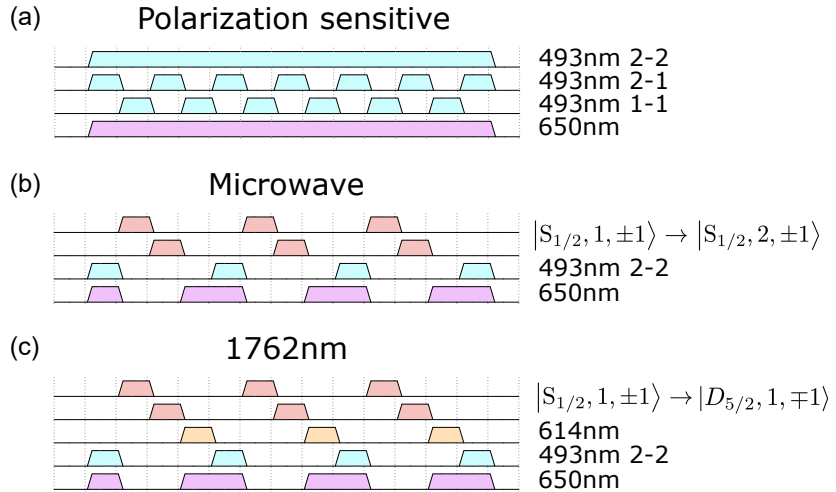
Error Source	Predicted Error ( $\times 10^{-5}$ )	
	$ 0\rangle$ State	$ 1\rangle$ State
$ 0\rangle$ state preparation	$<9.1$	—
$ 0\rangle \rightarrow  1\rangle$ transfer	—	$5.4 \pm 0.5$
Shelving infidelity	$\sim 0.1$	—
$D_{5/2}$ decay	$\sim 1.5$	—
Correlated errors	4.0	—
Subtotal (measured)	$14.7 \pm 2.4$	$4.2 \pm 1.3$
Total (measured)	$9.6 \pm 1.4$	

TABLE S-i. Error budget of 1762 nm scheme SPAM from Fig. 2(c) of the main text, same as Table 2 of the main text.

a Bayesian update assuming Poissonian-distributed counts and pre-determined fluorescence rates; each measurement begins with a uniform prior that is updated for each successive segment based on the registered counts and the known distributions and ends once enough segments have been analyzed to cross a confidence threshold, here  $10^{-6}$ , or all ten segments have been considered. Decays are then identified as shots that the threshold method determined to be bright but the Bayesian post-processing outcome was dark. This method can only catch decays that occur after an integration time sufficient to pass the confidence threshold, which varies shot to shot but is  $140 \mu\text{s}$  on average. We identify 7 such decays in this trial during the remaining  $210 \mu\text{s}$  which corresponds to roughly  $1.5 \times 10^{-5}$  error during the  $450 \mu\text{s}$  time the ion is shelved (measurement time plus second and third pulses of cabinet shelving) and is consistent with the published lifetime. While we implemented this step in post-processing, the analysis could be implemented in real-time to conclude measurement once a given confidence threshold is reached, both shortening average measurement time and cutting down on errors from decays.

A large error contribution comes from what we call “correlated errors” which show up as bright errors occurring in bunches as large as 20-30 trials in a row, and the fluorescence counts are lower than what we would expect for a “bright” ion. In taking SPAM data, we interleave trials preparing  $|0\rangle$  and  $|1\rangle$ , so these  $|0\rangle$  preparation errors also cause the corresponding  $|1\rangle$  counts to be erroneous. We believe that these errors are caused primarily by background collisions with our ion, but also by other experimental imperfections such as poor 493 nm laser locking and noise on our trapping electrodes. In this data set, we detect 40 such correlated bright errors, corresponding to a  $4.0 \times 10^{-5}$  error contribution.

The leftover error of  $9.1 \times 10^{-5}$  can be seen as an upper bound on the infidelity of the state preparation technique. In the absence of the errors due to imperfect experimental conditions listed here and considering only errors contributed by state preparation and  $D_{5/2}$  decay, our ideal SPAM infidelity would be  $5.3 \times 10^{-5}$ .



**Figure S4.** Experimental pulse sequences for (a) polarization state preparation with stroboscopically pulsed 493 nm sidebands, (b) microwave-assisted optical pumping, and (c) 1762 nm narrow-band optical pumping including the 493 nm flush beam. Axes are not to scale.

## STATE PREPARATION PULSE SEQUENCES

Figure S4 shows the pulse sequences we use for state preparation. Under polarization state preparation,  $\pi$ -polarized 493 nm light is applied to the ion to pump out all Zeeman states of  $S_{1/2}$  except the qubit state  $|0\rangle$  by taking advantage of the forbidden dipole selection rule  $|L, F, m_F = 0\rangle \leftrightarrow |L + 1, F, m_F = 0\rangle$ . The carrier at  $F = 2 \leftrightarrow F = 2$  (2-2) pumps out  $|S_{1/2}, F = 2, m_F \neq 0\rangle$ , while sidebands at 2-1 and 1-1 pump out  $|S_{1/2}, F = 2, m_F \neq \pm 2\rangle$  and  $|S_{1/2}, F = 1, m_F \neq 0\rangle$ , respectively. The sidebands must be pulsed stroboscopically to avoid mixing at the EOM, as the beat note drives the unwanted 1-2 transition. 650 nm light is applied throughout to repump any ions that fall into  $D_{3/2}$ .

In microwave-assisted optical pumping, 493 nm light with all polarizations flushes out the  $(S_{1/2}, F = 2)$  manifold, and 650 nm light is simultaneously applied to repump any ions that fall into  $D_{3/2}$ . Then, microwaves  $\pi$ -pulses move errors from  $F = 1$  up to  $F = 2$  by addressing  $|S_{1/2}, 1, \pm 1\rangle \rightarrow |S_{1/2}, 2, \pm 1\rangle$ , and these errors are then redistributed to  $F = 1$  with the next flush pulse.

In 1762 nm narrow-band optical pumping, a similar 493 nm flush pulse clears out the  $F = 2$  errors, but the  $F = 1$  errors are moved to  $D_{5/2}$  with 1762 nm  $\pi$ -pulses  $|S_{1/2}, 1, \pm 1\rangle \rightarrow |D_{5/2}, 1, \mp 1\rangle$  ( $\Delta m_F = \pm 2$ ). These errors are then deshelled with the 614 nm laser to  $(P_{3/2}, F = 0)$ , from which they predominantly decay back into  $(S_{1/2}, F = 1)$ .

---

\* [Fangzhao.An@Quantinuum.com](mailto:Fangzhao.An@Quantinuum.com)

† [Anthony.Ransford@Quantinuum.com](mailto:Anthony.Ransford@Quantinuum.com)

- [1] S. D. Erickson, J. J. Wu, P.-Y. Hou, D. C. Cole, S. Geller, A. Kwiatkowski, S. Glancy, E. Knill, D. H. Slichter, A. C. Wilson, *et al.*, [arXiv preprint arXiv:2112.06341](https://arxiv.org/abs/2112.06341) (2021).
- [2] Z. Zhang, K. J. Arnold, S. R. Chanu, R. Kaewuam, M. S. Safronova, and M. D. Barrett, [Phys. Rev. A](https://doi.org/10.1103/PhysRevA.101.062515) **101**, 062515 (2020).